Rev. Roum. Sci. Techn.– Électrotechn. et Énerg.
Vol. **68**, *1*, pp. 65–70, Bucarest, 2023

NONLINEAR FAULT TOLERANT CONTROL OF DUAL THREE-PHASE INDUCTION MACHINES BASED ELECTRIC VEHICLES

TOUFIK ROUBACHE[1], SOUAD CHAOUCH[2]

Keywords: Dual three-phase induction machine; Second-order sliding mode control; Sliding mode observer; Fault-tolerant control; Direct continue machine; Electric vehicle.

This paper proposes a robust fault-tolerant control (FTC) for the dual three-phase (DTP) induction machines under failures controlled by a higher-order sliding mode control strategy. However, the DTP induction machine is increasingly used because of better reliability and a supply division. A passive and an active FTC law have been designed and tested on DTP. The proposed method not only realizes the FTC and the fault elimination but also provides a possible solution for emulating a traction system using a direct continue machine (DCM) supplied by a four-quadrant chopper. Therefore, the emulation system is based on a controlled DCM, which imposes the same behavior of the mechanical power train of an electric vehicle to the DTP. Simulation results are given to verify the robustness and good performance of the proposed fault-tolerant control scheme.

1. INTRODUCTION

Various nonlinear control design approaches have recently been applied to the dual three-phase (DTP) induction machine control for better performance. This type of machine has some advantages, such as power segmentation, minimizing torque ripples, reducing rotor harmonic currents, and using the latter in wind projects, of which powers are of a few MW [1,2]. The DTP induction machines are used in several applications, especially those requiring high power, such as electric/hybrid vehicles, locomotive traction, and electric ship propulsion [3].

The nonlinear control of DTP machines is essential in an industrial environment, especially for electric drives [4]. One of the nonlinear control methods applied to DTP induction motor control is the second-order sliding mode (SOSM) control. In addition, the SOSM control has recently been paid much attention to [5–9]. Since robustness is the best advantage of an SMC, it has been widely employed to control nonlinear systems, especially those with model uncertainty and external disturbance [10,11]. These advantages justify applying this kind of control for the DTP. So, in this study, SOSM control based on a super-twisting algorithm is proposed.

For this reason, the SOSM has been suggested to obtain good steady state and dynamic behavior in the presence of faults, parameter variation, and external disturbances. The research and development of electric vehicles (EVs) have been significantly promoted to cope with the global energy crisis and environmental pollution. On the other hand, EVs are now the most promising and attractive alternative to combustion engine cars. This trend is caused by the very fast evolution of this technology [12–16]. As a result, several research has been recently devoted to studying fault tolerant control (FTC) applied to dual-stator induction machines.

Furthermore, problems related to FTC of descriptor systems have been widely studied. From the point of view of FTC strategies, the literature considers two main groups of techniques: passive (PFTC) and active (AFTC) approaches. PFTC refers to a class of fixed and robust controllers against the considered faults with no need for FDD [17,18]. Thus, AFTC utilizes diagnosis information from a fault detection and diagnosis (FDD) unit and employs control reconfiguration methods to guarantee the system's stability and achieve acceptable performance in the presence of considered faults [19]. In this context, a fault-tolerant control approach is proposed for a dual-stator induction machine in electric vehicle propulsion in case of the rotor and stator failure. Therefore, to highlight the FTCs, robust fault-tolerant control of the dual three-phase cage induction motor for an EV propulsion system is investigated based on the sliding mode observer, twisting algorithm, and higher order sliding mode. FTC schemes are characterized in this work by their capabilities, after fault occurrence, to recover performance close to the nominal desired performance. The simulated model results show compelling performances with introduced load disturbances and parameter variations, such as increased rotor and stator resistances. A detailed sliding mode controller of the DTP motor fed by two voltage source inverters integrating the proposed FTC is developed. The main contribution of this paper is to address the problem of passive and active fault tolerant control schemes for an EV system with an actuator fault is developed.

A sliding mode observer (SMO) is designed to estimate the state variables and fault signals. From these results, the proposed FTC and fault estimation algorithm are efficient. In conclusion, the main objective of this paper is to detect and compensate for actuator faults in the control loop. The rest of the paper is organized as follows: section 2 presents the mathematical model of the DTP induction motor. Machine faulty modeling and its failure modes are discussed in section 3. After that, the design of FTC schemes for a DTP is described in section 4. The simulation results are discussed and demonstrated in section 5, followed by the application of FTC to the emulator of electric vehicles in section 6. Finally, the conclusion and future works are presented in section 7.

2. DUAL THREE-PHASE INDUCTION MACHINE NONLINEAR MODEL

In this section, the mathematical model of a dual three-phase induction motor can be defined in a stationary (α,β) reference frame by the following state equation:

$$\dot{x}(t) = Ax(t) + Gu(t), \tag{1}$$

with

[1] Electrical Engineering Dep., University of Msila, Algeria, E-mail: toufik.roubache@gmail.com
[2] LSP-IE Laboratory, University of Batna 2, Algeria

$$\begin{cases} x(t)=\begin{bmatrix} i_{s\alpha1} & i_{s\beta1} & i_{s\alpha2} & i_{s\beta2} & \varphi_{r\alpha} & \varphi_{r\beta} \end{bmatrix}^T \\ G=\begin{bmatrix} g_1 & 0 & 0 & 0 & 0 & 0 \\ 0 & g_1 & 0 & 0 & 0 & 0 \\ 0 & 0 & g_2 & 0 & 0 & 0 \\ 0 & 0 & 0 & g_2 & 0 & 0 \end{bmatrix}^T \\ u(t)=\begin{bmatrix} u_{s\alpha1} & u_{s\beta1} & u_{s\alpha2} & u_{s\beta2} \end{bmatrix}^T \end{cases}. \quad (2)$$

The nonlinear matrix field $Ax(t)$ is described by the following equation:

$$\begin{cases} A_1x(t)=a_1\left(-R_{s1}i_{s\alpha1}-a_2i_{s\alpha2}-a_3\dot{\varphi}_{r\alpha}\right) \\ A_2x(t)=a_1\left(-R_{s1}i_{s\beta1}-a_2i_{s\beta2}-a_3\dot{\varphi}_{r\beta}\right) \\ A_3x(t)=a_4\left(-R_{s2}i_{s\alpha2}-a_2i_{s\alpha1}-a_3\dot{\varphi}_{r\alpha}\right) \\ A_4x(t)=a_4\left(-R_{s2}i_{s\beta2}-a_2i_{s\beta1}-a_3\dot{\varphi}_{r\beta}\right) \\ A_5x(t)=a_5\left(i_{s\alpha1}+i_{s\alpha2}\right)-a_6\varphi_{r\alpha}-a_7\varphi_{r\beta} \\ A_6x(t)=a_5\left(i_{s\beta1}+i_{s\beta2}\right)-a_6\varphi_{r\beta}+a_7\varphi_{r\alpha} \end{cases}. \quad (3)$$

The components of $Ax(t)$ are expressed as follows:

$$\begin{cases} a_1=\dfrac{1}{\sigma\left(L_m+L_{s1}\right)}, a_2=\dfrac{L_mL_r}{L_m+L_r}, a_3=\dfrac{L_m}{L_m+L_r}, \\ a_4=\dfrac{1}{\sigma\left(L_m+L_{s2}\right)}, a_5=\dfrac{L_m}{T_r}, a_6=\dfrac{1}{T_r}, a_7=\omega_r, \\ a_8=\dfrac{L_m}{J_mL_r}, a_9=\dfrac{-T_L}{J_m}, T_r=\dfrac{L_m+L_r}{R_r}, L_{s1}=L_{s2}=L_s, \\ g_1=a_1, g_2=a_4, \sigma=1-\dfrac{L_m^2}{\left(L_m+L_r\right)\left(L_m+L_s\right)}. \end{cases}$$

where R_{s1}, R_{s2}, R_r, L_s, L_r are stator/rotor resistances and inductances, respectively. L_m is the mutual inductance, J_m is the rotor inertia and T_L is the load torque.

3. FAULTY MODEL OF DTP INDUCTION MOTOR

In this section, the faulty model is applied to design a fault-tolerant controller for a dual induction motor in the presence of rotor and stator mechanical faults. The faults dealt with in this section can be summarized in the following two classes [19]:

- stator asymmetries, mainly due to static eccentricity.
- rotor asymmetries, mainly due to dynamic eccentricity.

Therefore, the stator currents in (α,β) axes could be modeled as follows:

$$\begin{cases} i_{s\alpha1}\rightarrow i_{s\alpha1}+A\sin\left(\omega_it+\varphi\right) \\ i_{s\beta1}\rightarrow i_{s\beta1}+A\cos\left(\omega_it+\varphi\right) \\ i_{s\alpha2}\rightarrow i_{s\alpha2}+A\sin\left(\omega_it+\varphi\right) \\ i_{s\beta2}\rightarrow i_{s\beta2}+A\cos\left(\omega_it+\varphi\right) \end{cases}, \quad (4)$$

in which $\omega_i=2\pi f_i$ where f_i is a specific frequency which will be for the faults caused by the stator and rotor asymmetries by $f_i=f_s$ and $f_i=\left(1\pm2k\dfrac{s_w}{\omega_s}\right)f_s$ respectively, with f_s is the supply frequency, $s_w=\omega_s-p\omega_m$ is defined as the slip angular frequency, and ω_s is stator angular frequency, while k is a positive integer. The amplitude A and phase φ in eq. (4) is unknown values depending on the fault's severity [20]. To point up the proposed control and use eq. (4) additional faults are injected into eq. (1).

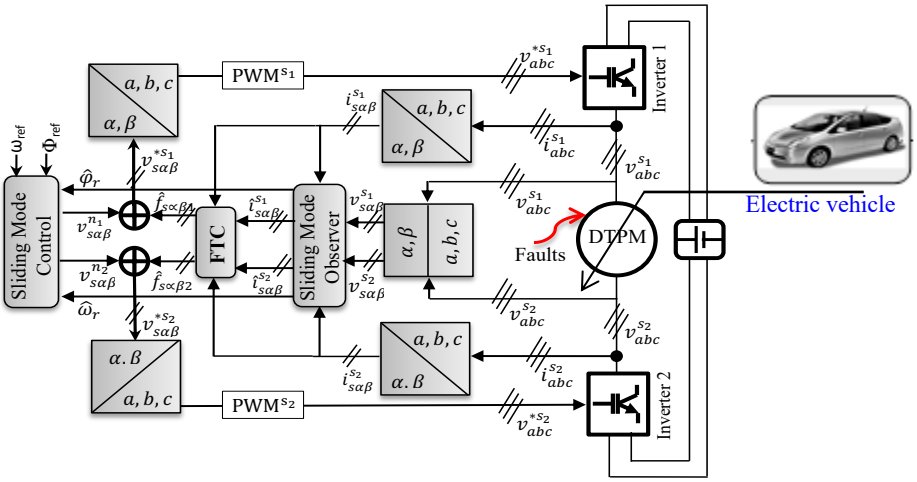

The machine's faulty model is expressed as follows:

$$\begin{cases} \dfrac{di_{s\alpha1}}{dt}=A_1x(t)+g_1u_{s\alpha1}+g_1f_{s\alpha1} \\ \dfrac{di_{s\beta1}}{dt}=A_2x(t)+g_1u_{s\beta1}+g_1f_{s\beta1} \\ \dfrac{di_{s\alpha2}}{dt}=A_3x(t)+g_2u_{s\alpha2}+g_2f_{s\alpha2} \\ \dfrac{di_{s\beta2}}{dt}=A_4x(t)+g_2u_{s\beta2}+g_2f_{s\beta2} \end{cases}. \quad (6)$$

where

$$\begin{cases} f_{s\alpha1}=f_{s\alpha2}=A\left[\omega_i\cos\left(\omega_it+\varphi\right)-\dfrac{1}{\tau_1}\sin\left(\omega_it+\varphi\right)\right] \\ f_{s\beta1}=f_{s\beta2}=-A\left[\omega_i\sin\left(\omega_it+\varphi\right)+\dfrac{1}{\tau_2}\cos\left(\omega_it+\varphi\right)\right], \\ \tau_1=\dfrac{1}{a_1R_{s1}}, \tau_2=\dfrac{1}{a_4R_{s2}} \end{cases} \quad (7)$$

4. FAULT-TOLERANT CONTROL STRATEGY

This section aims to design an active and a passive fault-tolerant controller to maintain the faulty system's stability,

robustness, and tracking performance. The structure of the fault-tolerant control for a DTPM is shown in Fig. 1. A fault-tolerant strategy is founded on the design of a nominal control law, fault estimation, and modification of the control law to compensate for the fault effect. However, two FTC types are used in this work.

4.1. PASSIVE FTC BASED SECOND ORDER SMC

Fault tolerance is obtained without changing the controller parameters. It is, therefore, called passive fault tolerance. In this case, passive fault-tolerant control uses one of the reliable control laws, which considers both fault-free and faulty situations. The first phase of the control design consists of numbers of the switching surfaces $S(x)$, two sliding surfaces are used and taken as follows:

$$\begin{cases} S_1(\omega_r) = k_1(\omega_{ref} - \omega_r) + (\dot{\omega}_{ref} - \dot{\omega}_r) \\ S_2(\phi_r) = k_2(\phi_{ref} - \phi_r) + (\dot{\phi}_{ref} - \dot{\phi}_r) \end{cases}, \tag{8}$$

with k_1 and k_2 are positive gains.

The corresponding derivative of (8) is given by:

$$\begin{cases} \dot{S}_1(\omega_r) = k_1(\dot{\omega}_{ref} - \dot{\omega}_r) + (\ddot{\omega}_{ref} - \ddot{\omega}_r) \\ \dot{S}_2(\phi_r) = k_2(\dot{\phi}_{ref} - \dot{\phi}_r) + (\ddot{\phi}_{ref} - \ddot{\phi}_r) \end{cases}. \tag{9}$$

After simplification calculates, derivatives of the sliding surfaces are given in matrix forms as follows:

$$\begin{bmatrix} \dot{S}_1 \\ \dot{S}_2 \end{bmatrix} = \begin{bmatrix} F_{1s1,2} \\ F_{2s1,2} \end{bmatrix} + \begin{bmatrix} -g_2\varphi_{r\beta} & g_1\varphi_{r\alpha} \\ g_1 L_m \varphi_{r\alpha} & g_2 L_m \varphi_{r\beta} \end{bmatrix} \begin{bmatrix} u_{1s1,2} \\ u_{2s1,2} \end{bmatrix}, \tag{10}$$

with

$$\begin{cases} F_{1s1,2} = (k_1 - a_1 - a_6)a_8(i_{s\beta 1,2}\varphi_{r\alpha} - i_{s\alpha 1,2}\varphi_{r\beta}) \\ -k_1 a_9 - a_7 a_8(i_{s\alpha 1,2}\varphi_{r\alpha} + a_3\phi_r) - k_1\dot{\omega}_{ref} - \ddot{\omega}_{ref} \\ F_{2s1,2} = 2a_6(a_6(2 + L_m\sigma) - k_2)\phi_r + 2a_6\Big(a_5\Big(i^2_{s\alpha 1,2} \\ + i^2_{s\beta 1,2}\Big) + (-3a_6 - a_1 + k_2)(i_{s\alpha 1,2}\varphi_{r\alpha} + i_{s\beta 1,2}\varphi_{r\beta}) \\ + pa_7(i_{s\beta 1,2}\varphi_{r\alpha} - i_{s\alpha 1,2}\varphi_{r\beta})\Big) - k_2\dot{\phi}_{ref} - \ddot{\phi}_{ref} \end{cases}$$

The condensed form of (10) is given by:

$$\dot{S} = F_s + Du. \tag{11}$$

Check the condition of Lyapunov stability $(S_i\dot{S}_i < 0)$, which must be:

$$\dot{S} = -\nu\text{sign}(S). \tag{12}$$

Equating (11) and (12), we have:

$$u = -D^{-1}\nu\text{sign}(S) - D^{-1}F_s. \tag{13}$$

The equivalent control law is given by:

$$\begin{bmatrix} u_{eq1s1,2} \\ u_{eq2s1,2} \end{bmatrix} = -D^1 \begin{bmatrix} F_{1s1,2} \\ F_{2s1,2} \end{bmatrix}. \tag{14}$$

The attractive control law is given by:

$$\begin{bmatrix} u_{c1s1,2} \\ u_{c2s1,2} \end{bmatrix} = -D^1 \begin{bmatrix} \nu_1 & 0 \\ 0 & \nu_2 \end{bmatrix} \begin{bmatrix} \text{sign}(S_1) \\ \text{sign}(S_2) \end{bmatrix}, \tag{15}$$

where

$$\begin{bmatrix} \nu_1 \\ \nu_2 \end{bmatrix} = \begin{bmatrix} \vartheta_1 + \delta_1|S_1|^\rho \\ \vartheta_2 + \delta_2|S_2|^\rho \end{bmatrix}, \tag{16}$$

with

$$\begin{cases} \vartheta_i > \dfrac{\mathrm{H}}{k_m} \\ \delta_i^2 \geq \dfrac{4\mathrm{H}}{k_m^2}\dfrac{k_M(\vartheta_i + \mathrm{H})}{k_m(\vartheta_i - \mathrm{H})} \\ 0 < \rho \leq 0.5, i = 1,2 \end{cases} \tag{17}$$

where ϑ_i, δ_i, H, k_m, and k_M are positive gains and constants, respectively [21].

The global control ensuring both $(S_i = 0)$ and $(S_i\dot{S}_i < 0)$ is given by:

$$u_n = \begin{bmatrix} u_{1s1,2} \\ u_{2s1,2} \end{bmatrix} = \begin{bmatrix} u_{eq1s1,2} \\ u_{eq2s1,2} \end{bmatrix} + \begin{bmatrix} u_{c1s1,2} \\ u_{c2s1,2} \end{bmatrix}. \tag{18}$$

4.2. ACTIVE FTC-BASED SLIDING MODE OBSERVER

In this case, the whole state of the system was considered accessible for measurement and completely controllable. The rotor flux cannot be easily measured in practical applications. The complete structure of the observer is based on a sliding mode. A sliding mode observer is synthesized to systematically reconstruct system states and machine faults. On the other hand, the objective is to enforce the observation error to converge to zero by tracking the system output variables.

The proposed sliding mode observer for state and fault estimation can be constructed as follows:

$$\begin{cases} \dot{\hat{x}}_i = A_{11}\hat{x}_i + A_{12}\hat{x}_\Phi B_1 u + k_i\text{sign}(\hat{i}_s - i_s) \\ \dot{\hat{x}}_\phi = A_{21}\hat{x}_i + A_{22}\hat{x}_\Phi + k_\phi\text{sign}(\hat{i}_s - i_s) \end{cases}, \tag{19}$$

where

$$\begin{cases} A_{11} = a_1 I, A_{12} = a_3\left(T_r^{-1}I + \omega_r J_m\right), B_1 = g_1 I, A_{21} = a_6 I, \\ A_{22} = -\left(T_r^{-1}I + \omega_r J\right), I = \begin{bmatrix} 1 & 0 \\ 0 & 1 \end{bmatrix}, J = \begin{bmatrix} 0 & -1 \\ 1 & 0 \end{bmatrix} \end{cases}.$$

The estimated stator currents and flux components can be expressed by:

$$\begin{cases} \hat{x}_i = \begin{bmatrix} \hat{i}_{s\alpha} & \hat{i}_{s\beta} \end{bmatrix}^T \\ \hat{x}_\phi = \begin{bmatrix} \hat{\phi}_{r\alpha} & \hat{\phi}_{r\beta} \end{bmatrix}^T \end{cases}. \tag{20}$$

Let us define the observer error as follows:

$$\bar{e}(t) = \bar{x}(t) - \hat{x}(t) = \begin{bmatrix} e(t) & e_f(t) \end{bmatrix}^T. \tag{21}$$

where $e(t)$ and $e_f(t)$ are the state estimation error and the sensor fault estimation error, respectively. Then, the error dynamics are given by:

$$\begin{cases} \dot{\bar{e}}_{s\alpha1}(t) = (a_1 - a_1 R_{s1}) e_{s\alpha1} + (a_1 - a_1 a_2) e_\phi \\ + k_{i\alpha} \text{sign}(e_{s\alpha1}) - f_{s\alpha1} \\ \dot{\bar{e}}_{s\beta1}(t) = (a_1 - a_1 R_{s1}) e_{s\beta1} + (a_1 - a_1 a_2) e_\phi \\ + k_{i\beta} \text{sign}(e_{s\beta1}) - f_{s\beta1} \\ \dot{\bar{e}}_{s\alpha2}(t) = (a_4 - a_4 R_{s2}) e_{s\alpha2} + (a_4 - a_4 a_2) e_\phi \\ + k_{i\alpha} \text{sign}(e_{s\alpha2}) - f_{s\alpha2} \\ \dot{\bar{e}}_{s\beta2}(t) = (a_4 - a_4 R_{s2}) e_{s\beta2} + (a_4 - a_4 a_2) e_\phi \\ + k_{i\beta} \text{sign}(e_{s\beta2}) - f_{s\beta2} \end{cases}, \quad (22)$$

where $k_{i\alpha}$ and $k_{i\beta}$ are strictly positive constants, that the asymptotic convergence of the estimation errors to zero is guaranteed. This is done by introducing the Lyapunov function candidate:

$$V = \frac{1}{2}\left(e_{s\alpha1}^2 + e_{s\beta1}^2 + e_{s\alpha2}^2 + e_{s\beta2}^2\right). \quad (23)$$

The derivative of (23) concerning time is:

$$\dot{V} = e_{s\alpha1}\dot{e}_{s\alpha1} + e_{s\beta1}\dot{e}_{s\beta1} + e_{s\alpha2}\dot{e}_{s\alpha2} + e_{s\beta2}\dot{e}_{s\beta2}. \quad (24)$$

Choosing the functions $\dot{V}_1, \dot{V}_2, \dot{V}_3$, and $\dot{V}_4$ as follows:

$$\begin{cases} \dot{V}_1 = e_{s\alpha1}\dot{e}_{s\alpha1} = e_{s\alpha1}\left[(a_1 - a_1 R_{s1}) e_{s\alpha1}\right. \\ \left. + (a_1 - a_1 a_2) e_\phi + k_{i\alpha} \text{sign}(e_{s\alpha1}) - f_{s\alpha1}\right] \\ \dot{V}_2 = e_{s\beta1}\dot{e}_{s\beta1} = e_{s\beta1}\left[(a_1 - a_1 R_{s1}) e_{s\beta1}\right. \\ \left. + (a_1 - a_1 a_2) e_\phi + k_{i\beta} \text{sign}(e_{s\beta1}) - f_{s\beta1}\right] \\ \dot{V}_3 = e_{s\alpha2}\dot{e}_{s\alpha2} = e_{s\alpha2}\left[(a_4 - a_4 R_{s2}) e_{s\alpha2}\right. \\ \left. + (a_4 - a_4 a_2) e_\phi + k_{i\alpha} \text{sign}(e_{s\alpha2}) - f_{s\alpha2}\right] \\ \dot{V}_4 = e_{s\beta2}\dot{e}_{s\beta2} = e_{s\beta2}\left[(a_4 - a_4 R_{s2}) e_{s\beta2}\right. \\ \left. + (a_4 - a_4 a_2) e_\phi + k_{i\beta} \text{sign}(e_{s\beta2}) - f_{s\beta2}\right] \end{cases}. \quad (25)$$

During the convergence mode, the conditions $\dot{V}_1 < 0$, $\dot{V}_2 < 0$, $\dot{V}_3 < 0$, and $\dot{V}_4 < 0$ must be verified.

The sliding mode will occur, *i.e.*, $e_{s\alpha1} = \dot{e}_{s\alpha1} = 0$, $e_{s\beta1} = \dot{e}_{s\beta1} = 0$, $e_{s\alpha2} = \dot{e}_{s\alpha2} = 0$, and $e_{s\beta2} = \dot{e}_{s\beta2} = 0$. Then, the faults can be estimated. Therefore, the eq. (25) becomes:

$$\begin{cases} (a_1 - a_1 a_2) e_\phi + k_{i\alpha} \text{sign}(e_{s\alpha1}) - f_{s\alpha1} = 0 \\ (a_1 - a_1 a_2) e_\phi + k_{i\beta} \text{sign}(e_{s\beta1}) - f_{s\beta1} = 0 \\ (a_4 - a_4 a_2) e_\phi + k_{i\alpha} \text{sign}(e_{s\alpha2}) - f_{s\alpha2} = 0 \\ (a_4 - a_4 a_2) e_\phi + k_{i\beta} \text{sign}(e_{s\beta2}) - f_{s\beta2} = 0 \end{cases}. \quad (26)$$

Equation (26) shows that e_ϕ converges to zero as $t \to \infty$, and the estimates of the faults are given by

$$\begin{cases} \hat{f}_{s\alpha1} = k_{i\alpha} \text{sign}(e_{s\alpha1}) \\ \hat{f}_{s\beta1} = k_{i\beta} \text{sign}(e_{s\beta1}) \\ \hat{f}_{s\alpha2} = k_{i\alpha} \text{sign}(e_{s\alpha2}) \\ \hat{f}_{s\beta2} = k_{i\beta} \text{sign}(e_{s\beta2}) \end{cases}. \quad (27)$$

To verify the system stability, coefficients $k_{i\alpha}$ and $k_{i\beta}$ must be strictly positive.

5. SIMULATION RESULTS

In this section, different simulations will be performed to reconstruct the faults in the machine using the passive and active fault tolerant control. The flux reference value is set to 1 Wb for DTPM. The nominal parameters of the DTP induction motor are listed in Table 1.

Table 1
DTP induction motor parameters

Parameters	Value	Parameters	Value
P_n	4 Kw	L_m	0.3672 H
f_a	50 Hz	L_r	0.006 H
R_{s1}=R_{s2}	3.72 Ω	J_m	0.0625 kg.m^2
R_r	3.72 Ω	k_f	0.001 N.m.s/rd
L_{s1}=L_{s2}	0.022 H	P	1

5.1. SIMULATION TESTING RESULTS BASED PFTC

Using the nominal algorithm above, the passive FTC controller can be simulated and tested. In this case, at start-up, the DTP machine operates with the nominal values of these parameters, and between the time t = 1 s and 2 s, a step of 50 % of rotor and stator resistances is applied separately. Figures 2 and 3 show the robustness of the DTP induction motor-based sliding mode control. Figure 2 shows the reference and the real rotor speed of robustness for speed DTP induction motor when the rotor speed reference is switched between [1432;-14332;477;0] rpm. This figure shows the response and the zoom rotor speed. It is observed that the rotor speed can track its reference value with small oscillation and is not affected by a 50 % increase in the rotor and stator resistances.

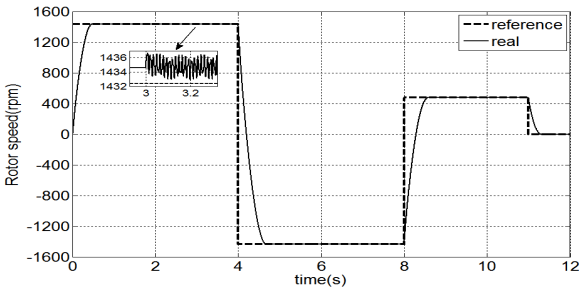

Fig. 2 – Rotor speed robustness via passive FTC and zoom around fault appearance at t = 3 s.

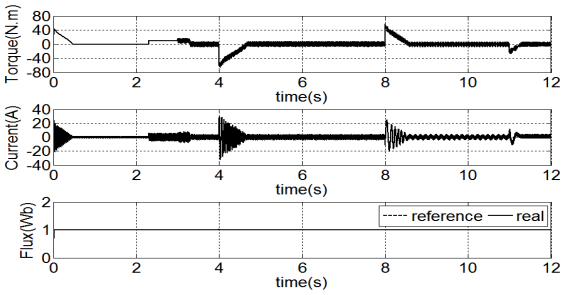

Fig. 3 – Dynamic output responses via passive fault tolerant control

5.2. SIMULATION TESTING RESULTS BASED AFTC

Based on the sliding mode observer, the active fault tolerant control (AFTC) system has also been tested successfully, as shown in Figs. 4-5. Figure 4 shows the reference, the real, and the estimated rotor speed of robustness for the speed DTP induction machine. In all simulation testing results, the load torque was applied and omitted between [2.2;3.2] s. The estimated rotor speed would coincide precisely with the real rotor speed even if there was the load torque application instant. From these results, it is shown that the proposed active FTC algorithm has good performance. The robustness of the active FTC has been proven to be stronger based on the comparison of Figs. 2-3 (PFTC) and Figs. 4-5 (AFTC), in the same environment, active FTC is more robust than passive FTC in handling extra disturbances. The rotor flux starts from zero and increases to the rated constant value of 1 Wb. SMO exhibits strong robustness to motor parameter variations, such as stator and rotor resistances. The SMO with FTC demonstrates excellent performance under failure, which confirms that active FTC shows strong robustness to parameter variations and faults.

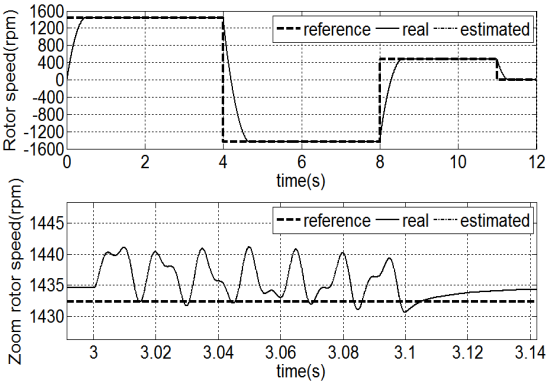

Fig. 4 – Rotor speed (upper plot) robustness via active FTC and zoom around fault appearance at t = 3 s (lower plot).

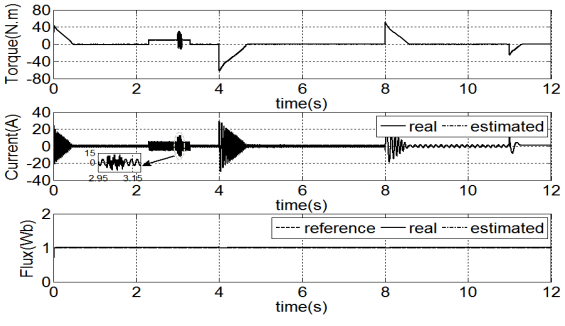

Fig. 5–Dynamic output responses via active fault tolerant control

6. DYNAMIC EMULATOR OF EV APPLICATION

My interest in this mechanical system is motivated by the similarity between its dynamic properties and those of several real-world engineering applications. Using the classical configuration of an electric vehicle (EV), the driving wheels are used two separate DTP induction motors drive (DTPM). On the other hand, the dynamic vehicle model is given in [22]. The proposed scheme of the EV emulator is given in Fig. 6. The role of this vehicle emulator is to replace the real vehicle while keeping the same behavior when it receives the same speed reference to be able to test any case. The aerodynamics and mechanics characteristic of the EV model has been reproduced perfectly by a separately excited dc machine (DCM) with a dc/dc converter.

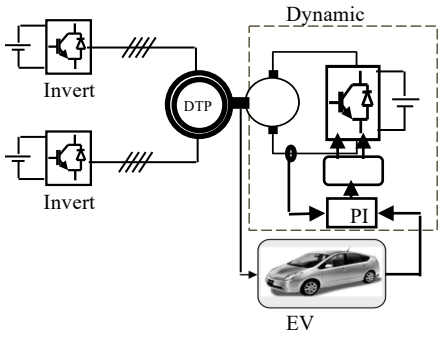

Fig. 6 – Electric vehicle

Simulation results of EV emulator with DTPM are presented in Fig. 7 and Fig. 8. The Figs. 7-8 illustrate the reference, the rotor flux (a), the real and the emulated of rotor speed (b) with the emulated torque (c), and the linear speed of EV (d). In addition, variation of 50 % of the stator and rotor resistances between the time t = 4 s and t = 5 s with variable speed reference are introduced after the faults occurred at t = 6 s. Two levels of simulation results will be presented here: firstly, Fig. 7 shows the simulation results of PFTC, and secondly, Fig. 8 shows the obtained simulation results of AFTC. In other words, the simulation results of PFTC in Fig. 7 do not show good rotor speed tracking. To improve rotor speed tracking, we used the AFTC. The simulation results displayed in Fig. 8 show that the active FTC is still efficient. In addition, SMO with FTC can provide even better performance under faulty conditions. Moreover, the obtained results tests proved that both FTCs structures respond well to a sudden change in the speed and parameter variations.

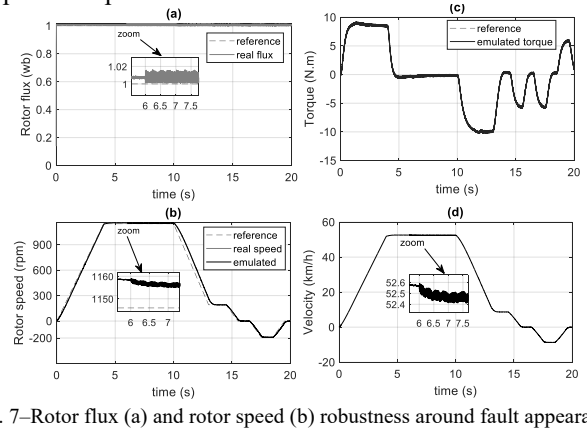

Fig. 7–Rotor flux (a) and rotor speed (b) robustness around fault appearance at t = 6 s, emulated torque (c) and EV speed (d) via PFTC.

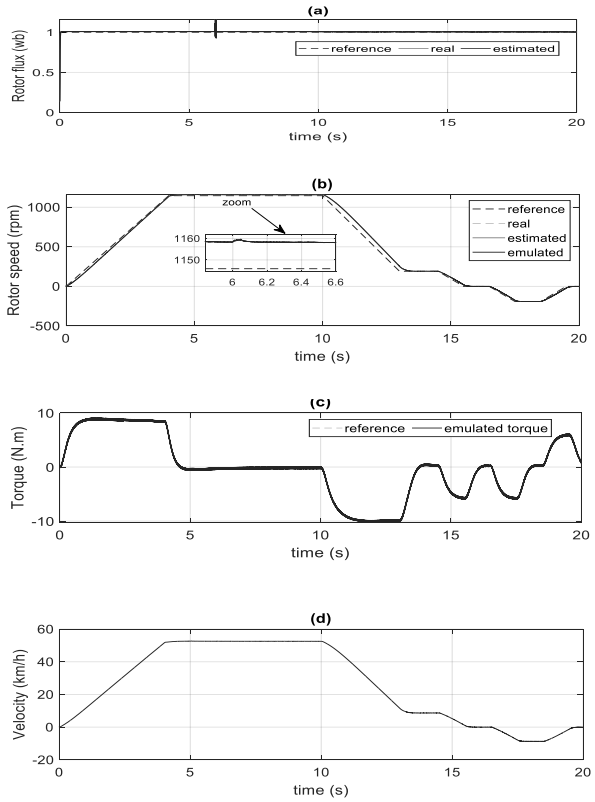

Fig. 8 – Rotor flux (a) and rotor speed (b) robustness around fault appearance at t = 6 s, emulated torque (c) and EV speed (d) via AFTC.

7. CONCLUSION

This paper proposes an FTC strategy for EVs using a DTP machine-based drive system. For that purpose, we have presented two types of nonlinear controls, a passive and an active FTC consensus. Both controllers worked properly. We can mention good results for all nonlinear controls. Then the active FTC gives better results when its performance increases, especially for rotor flux, rotor speed, and rotor with stator resistances variation. In this paper, we would like to highlight the concept of an emulator for electric vehicle characteristics that also provide good precision. It is shown by simulation with the different tests to prove the robustness of our proposed approach. Further investigations will regard the proof of the stability of the complete fault-tolerant schemes. As one of our future works, the proposed control will be developed, implemented, and tested.

Received on 17 December 2021

REFERENCES

1. S. Lekhchine, T. Bahi, Y. Soufi, *Indirect rotor field oriented control based on fuzzy logic controlled double star induction machine*, Electrical Power and Energy Systems, **57**, pp. 206–211 (2014).
2. A. Meroufel, S. Massoum, A. Bentaallah, P. Wira, F. Belaimeche, A. Massoum, *Double star induction motor direct torque control with fuzzy sliding mode speed controller*, Rev. Roum. Sci. Techn. – Électrotechn. Et Énerg., **62**, *1*, pp. 31–35 (2017).
3. K. Sahraoui, K. Katiaand A. Ameur, *A robust sensorless iterated extended kalman filter for electromechanical drive state estimation*, Electrotehnica Electronica Automatica, **65**, *2*, pp. 46–53 (2017).
4. Z. Tir, Y. Soufi, M.N. Hashemnia, O. Malik, K. Marouani, *Fuzzy logic field oriented control of double star induction motor drive*, Electrical Engineering, **99**, *2*, pp. 495–503 (2017).
5. B. Beltran, M. Benbouzid, T. Ahmed-Ali, *Second-order sliding mode control of a doubly fed induction generator driven wind turbine*, IEEE Transactions on Energy Conversion, **27**, *2*, pp. 261–269 (2012).
6. S. Ding, J. Park, C.C. Chen, *Second-order sliding* mode controller *design with output constraint*, Automatica, **112**, *2*, (2020).
7. Y. Bendjeddou, A. Deboucha, L. Bentouhami, E. Merabet, R. Abdessemed, *Super twisting sliding mode approach applied to voltage orientated control of a stand-alone induction generator*, Protection and Control of Modern Power Systems, **6**, *18*, (2021).
8. S. Benelghali, M. Benbouzid, T. Ahmed-Ali, J.F. Charpentier, *High-order sliding mode control of a marine current turbine driven doubly-fed induction generator*, IEEE Journal of Oceanic Engineering, **35**, *2*, pp. 402–411 (2010).
9. A. Ounissi, A. Kaddouri, M.S. Aggoun, R. Abdessemed, *Second order sliding mode controllers of micropositioning stage piezoelectric actuator with colman-hodgdon model parameters*, Rev. Roum. Sci. Techn. – Électrotechn. Et Énerg., **67**, *1*, pp. 41–46 (2022).
10. S.J. Huang, H.Y. Chen, *Adaptive sliding controller with self-tuning fuzzy compensation for vehicle suspension control*, *Science Direct,* Elsevier, Mechatronics, **16**, pp. 607–622 (2006).
11. Z. Yan, C. Jin, V.I. Utkin, *Sensorless sliding-mode control of induction motors*, IEEE Trans. Ind. Electron, **47**, *6*, pp. 1286–1297 (2005).
12. J. Hu, D. Yin, Y. Hori, *Fault-tolerant traction control of electric vehicles*, Control Engineering Practice, **19**, *2*, pp. 204–213 (2011).
13. B. Tabbache, A. Kheloui, M. Benbouzid, *An adaptive electric differential for electric vehicles motion stabilization*, IEEE Transactions Vehicular Technology, **60**, *1*, pp. 104–110 (2011).
14. R. Castro, R. Araujo, D. Freitas, *Wheel slip control of EVs based on sliding mode technique with conditional integrators*, IEEE Transactions on Industrial Electronics, **60**, *8*, pp. 3256–3271 (2013).
15. K. Nam, H. Fujimoto, Y. Hori, *Advanced motion control of electric vehicles based on robust lateral tire force control via active front steering*, IEEE Transactions on Mechatronics, **19**, *1*, pp. 289–299 (2014).
16. A. Derbane, B. Tabbache, A. Ahriche, *A fuzzy logic approach based direct torque control and five-leg voltage source inverter for electric vehicle powertrains*, Rev. Roum. Sci. Techn. – Électrotechn. Et Énerg., **66**, *1*, pp. 15–20 (2021).
17. Y.M. Zhang, J. Jiang, *Bibliographical review on reconfigurable fault-tolerant control systems*, Annu. Rev. Control, **32**, pp. 229–252 (2008).
18. M. Benosman, K.Y. Lum, *Passive actuators fault-tolerant control for affine nonlinear systems*, IEEE Transactions on Control Systems Technology, **18**, *1*, pp. 152–163 (2010).
19. J. Cieslak, D. Henry, A. Zolghadri, P. Goupil, *Development of an active fault tolerant flight control strategy*, AIAA Journal of Guidance, Control, and Dynamics, **31**, *1*, pp. 135–147 (2008).
20. C. Bonivento, A. Isidori, L. Marconi, A. Paoli, *Implicit fault-tolerant control: Application to induction motors*, Automatica, **40**, 3, pp. 355–371 (2004).
21. Z. Zhao, H. Gu, J. Zhang, G. Ding, *Terminal sliding mode control based on super-twisting algorithm*, Journal of Systems Engineering and Electronics, **28**, *1*, pp. 145–150 (2016).
22. T. Roubache, S. Chaouch, M.S. Nait-Said, *Sensorless fault-tolerant control of an induction motor based electric vehicle*, J Electr Eng Technol, **11**, *5*, pp. 1423–1432 (2016).